

Manipulating positions of CH···N in acceptors of pyrimidine-pyridine hybrids for highly efficient sky-blue thermally activated delayed fluorescent OLEDs

Qing Zhang, Shuaiqiang Sun, Xialei Lv, Wei Liu, Hongxia Zeng, Runda Guo, Shaofeng Ye, Panpan Leng, Songpo Xiang, Lei Wang*

Wuhan National Laboratory for Optoelectronics, Huazhong University of Science and Technology, Wuhan, 430074, P. R. China

Email: wanglei@mail.hust.edu.cn

Computational Details

The geometrical and electronic properties were computed using the Gaussian 09 program package. The ground-state geometry was optimized using density functional theory (DFT) and timed dependent DFT (TD-DFT) calculations using the B3LYP hybrid functional at the basis set level of 6-31G(d). Molecular orbitals were visualized using Gaussian view.

Measurement instruments

¹H NMR and ¹³C NMR spectra were obtained through a Bruker-AF301 AT spectrometer. Mass spectrometry were carried out on a Bruker-Daltonics microflex LT/SH mass spectrometer. Elemental analyses of carbon, hydrogen, and nitrogen were performed on an Elementar (Vario Micro cube) analyzer. Single crystal X-ray diffraction intensity data was recorded on a XtaLAB PRO MM007HF machine at 100 K with graphite-monochromatized Cu K α radiation ($\lambda = 1.54184 \text{ \AA}$). The multiscan method was used for absorption corrections. The structures were solved by direct method and were refined with SHELXL-2014/7.¹ CCDC numbers 1858076 and 1858077 for **DPAc-4PyPM** and **DPAc-6PyPM**, respectively. TGA was undertaken using a PerkinElmer Instruments (Pyris1 TGA) under the nitrogen environment at a heating rate of 10 °C min⁻¹ from RT to 600 °C. The temperature at 5% weight loss was used as the decomposition temperature (T_d). DSC was conducted on a PE Instruments

DSC 2920 unit at a heating rate of $10\text{ }^{\circ}\text{C min}^{-1}$ from $50\text{ }^{\circ}\text{C}$ to $200\text{ }^{\circ}\text{C}$ under a nitrogen atmosphere. The glass transition temperature (T_g) was determined from the second heating scan. Cyclic voltammetry (CV) was carried out on a computer-controlled EG&G Potentiostat/Galvanostat model 283 at room temperature with a conventional three electrode cell, which consisted of a Pt carbon working electrode of 2 mm in diameter, a platinum wire counter electrode, and an Ag/AgNO₃ (0.1 M) reference electrode. The supporting electrolyte was 0.1 M tetrabutylammonium hexafluorophosphate (Bu₄NPF₆) in CH₂Cl₂ and N,N-Dimethylformamide (DMF) solution. The onset potential was determined from the intersection of two tangents drawn at the rising and background current of the cyclic voltammogram. All solutions were purged with a nitrogen stream for 10 min before measurement. UV-Vis absorption spectra were recorded on a Shimadzu UV-VIS-NIR Spectrophotometer (UV-3600). Fluorescence measurements were carried out using Hitachi F-7000 fluorescence spectrophotometer and Edinburgh instruments (FLS920 spectrometers). Absolute PLQYs were obtained using a Quantaaurus-QY measurement system (C11347-11, Hamamatsu Photonics). Time-resolved spectra were obtained by exciting the sample with a Nd:yttrium aluminium garnet (YAG) laser (EKSPLA), 10 Hz, 355 nm. Sample emission was directed onto a spectrograph and gated intensified charged couple device (iCCD) camera (Stanford Computer Optics), more details about the nanosecond time-resolved spectroscopy can be found elsewhere.²

Device fabrication and measurement

The device fabrication and measurement are nearly identical with our previous reports.^{3, 4} Indium tin oxide (ITO) with a sheet resistance of $15\text{ }\Omega\text{ square}^{-1}$ was used as the substrate. Prior to use, the ITO glass substrates were pre-cleaned carefully and treated by oxygen plasma for 5 min before device fabrication. Then the sample was transferred to the deposition system. All organic layers and MoO₃ were deposited at a rate of $1\text{ }\text{\AA}\text{ s}^{-1}$, and subsequently LiF was deposited at $0.2\text{ }\text{\AA}\text{ s}^{-1}$ and then capped with Al (ca. $4\text{ }\text{\AA}\text{ s}^{-1}$) through a shadow mask in a vacuum of $2\times 10^6\text{ Torr}$. For all the OLEDs, the emitting areas were determined by the overlap of two electrodes as 0.09 cm^2 . The EL spectra,

CIE coordinates and $J-V-L$ curves of the devices were measured with a PHOTO RESEARCH SpectraScan PR 655 photometer and a KEITHLEY 2400 SourceMeter constant current source. The EQE values were calculated according to previously reported methods. All measurements were carried out at room temperature under ambient conditions.

Dynamic Rate Constant Calculation

The evaluation of exciton dynamic rate constants was calculated by equation S1-S8.^{5, 6}

$$k_F = \phi_F / \tau_p \quad \text{Equation S1}$$

$$\phi = k_F / (k_F + k_{IC}) \quad \text{Equation S2}$$

$$\phi_F = k_F / (k_F + k_{IC} + k_{ISC}) \quad \text{Equation S3}$$

$$\phi_{IC} = k_{IC} / (k_F + k_{IC} + k_{ISC}) \quad \text{Equation S4}$$

$$\phi_{ISC} = 1 - \phi_F - \phi_{IC} = k_{ISC} / (k_F + k_{IC} + k_{ISC}) \quad \text{Equation S5}$$

$$k_{TADF} = \phi_{TADF} / \phi_{ISC} \tau_d \quad \text{Equation S6}$$

$$k_{TADF} = (1/3) [k_F \exp(\dots) (-\Delta E_{ST}/RT)] \quad \text{Equation S7}$$

$$k_{RISC} = k_F k_{TADF} / (k_F - k_{ISC}) \quad \text{Equation S8}$$

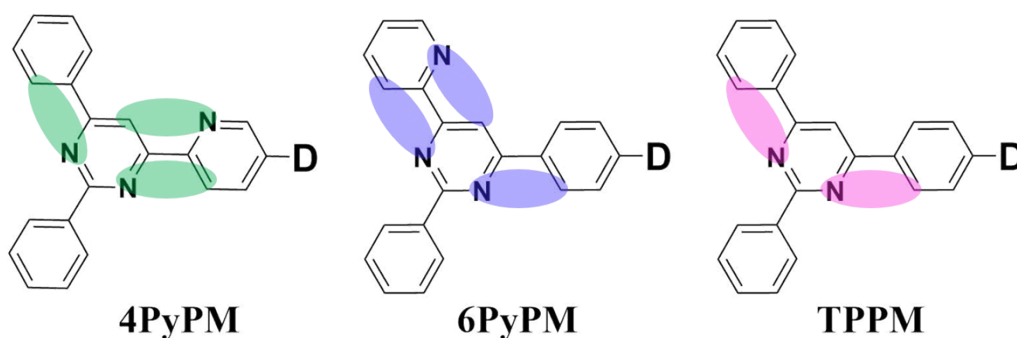


Fig. S1 The strategy of constructing CH···N intramolecular hydrogen-bonding interactions.

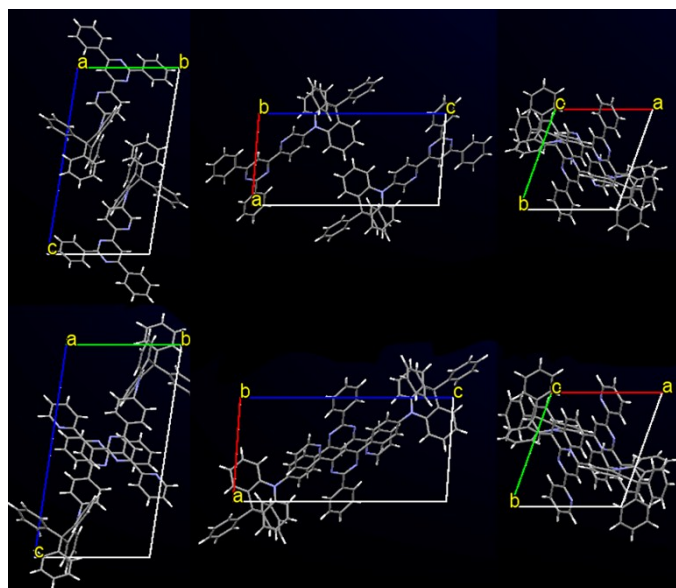


Fig. S2 The packing diagrams from axis direction of *a* (left), *b* (middle) and *c* (right) for **DPAC-4PyPM** (upper) and **DPAC-6PyPM** (below), respectively.

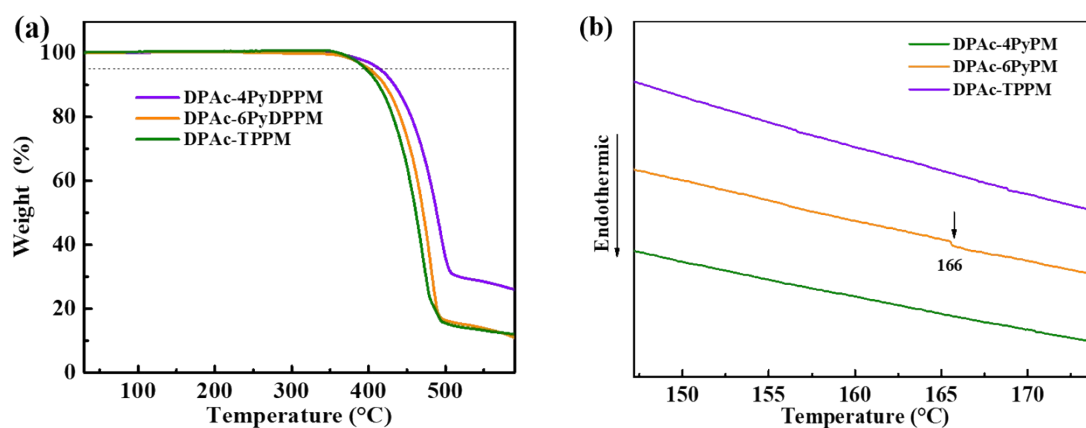


Fig. S3 (a) The TGA and (b) DSC thermograms of **DPAC-4PyPM**, **DPAC-6PyPM** and **DPAC-TPPM** recorded at a heating rate of $10\text{ }^{\circ}\text{C min}^{-1}$.

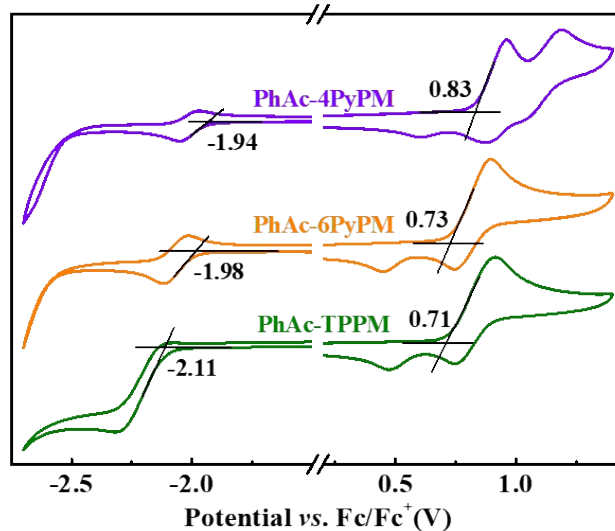


Fig. S4 Cyclic voltammogram of **DPAC-4PyPM**, **DPAC-6PyPM**, **DPAC-TPPM**.

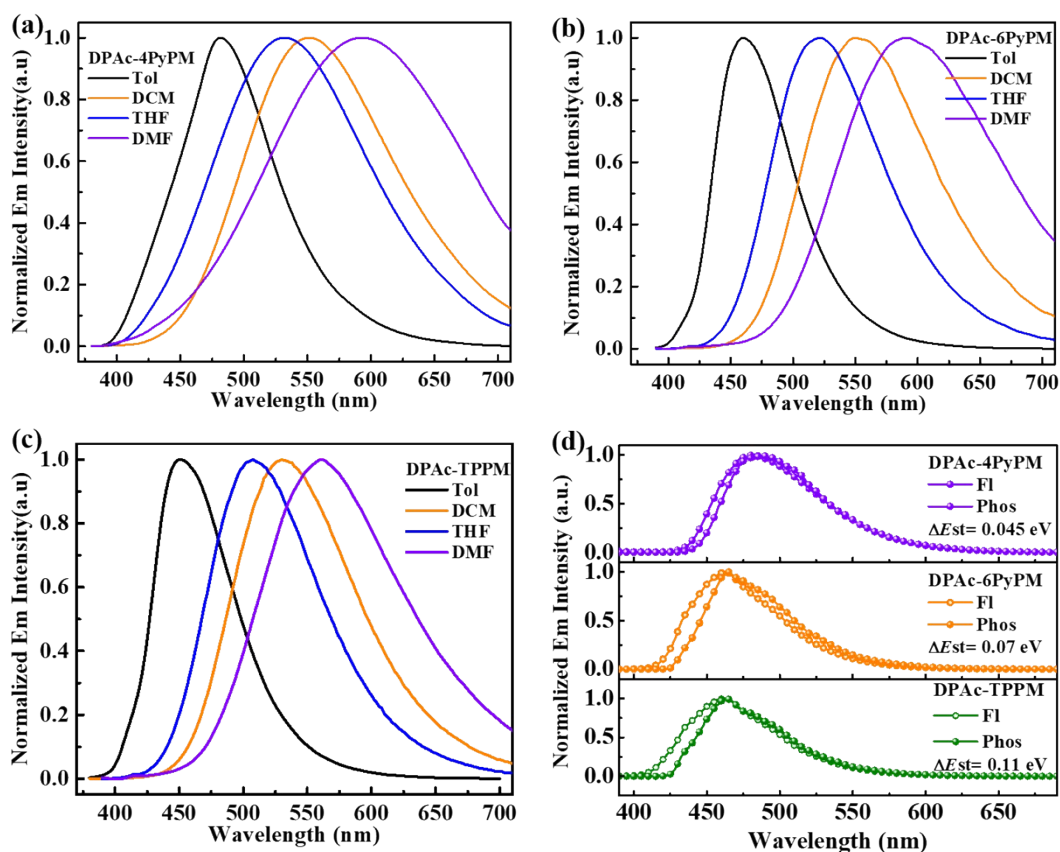


Fig. S5 (a)-(c) The fluorescence spectra of **DPAc-4PyPM**, **DPAc-6PyPM** and **DPAc-TPPM** in different solvents at room temperature and **(d) phosphorescence (Phos) spectra of DPAc-4PyPM, DPAc-6PyPM and DPAc-TPPM in 2-methyl-tetrahydrofuran at 77 K and their ΔE_{st} values.**

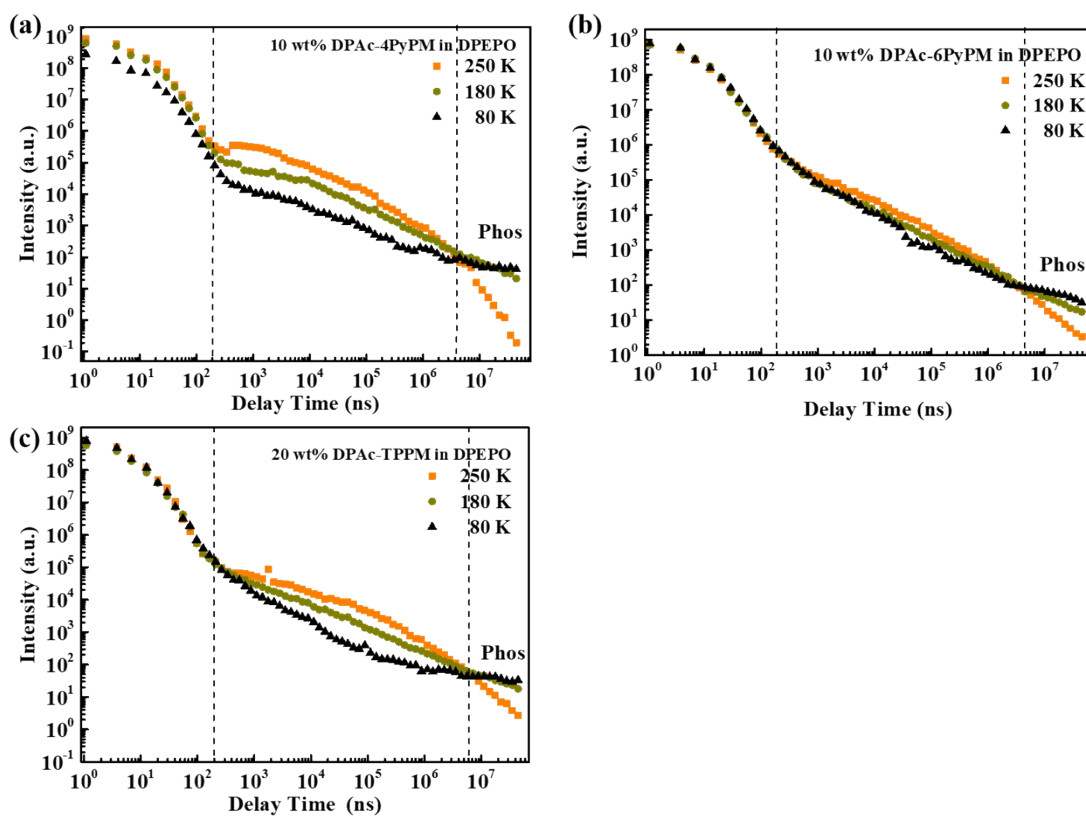


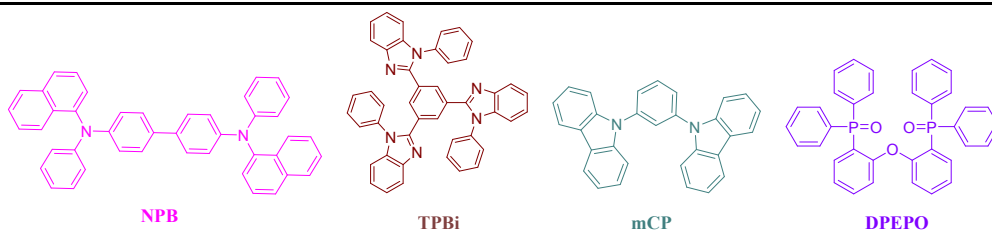
Fig. S6 The temperature-dependent transient PL decay spectra of 10 wt% (a) **DPAc-4PyPM**, (b) **DPAc-6PyPM** and 20 wt% **DPAc-TPPM** in DPEPO from 80 K to 250 K.

Table S1 The detail kinetic parameters

Compounds	ϕ_{PL}^a (%)	ϕ_{F}^b (%)	ϕ_{TADF}^b (%)	k_{F}^c (10^7 s^{-1})	k_{ISC}^c (10^7 s^{-1})	k_{IC}^c (10^6 s^{-1})	k_{TADF}^c (10^4 s^{-1})	k_{RISC}^c (10^5 s^{-1})	ΔE_{st}^c (eV)
DPAc-4PyPM	86	47.30	38.70	3.56	3.39	5.80	3.79	7.80	0.14
DPAc-6PyPM	83	54.95	28.05	4.91	3.02	10.0	5.10	1.33	0.14
DPAc-TPPM	70	46.27	23.73	5.77	4.23	24.7	1.86	0.69	0.17

^a The total PLQYs of emitters doped into DPEPO films under oxygen-free conditions at room temperature; ^b calculated by integral area of **Fig. 4b**; ^c calculated using equations S1-S8. (*x* wt.% emitters doped into DPEPO films; 10 wt.% for **DPAc-4PyPM** and **DPAc-6PyPM**; 20 wt.% for **DPAc-TPPM**.)

Device A: ITO/ M_2O_3 (10)/ NPB (60)/ mCP (15)/ DPEPO: 10 wt.% **DPAc-4PyPM** (20)/ DPEPO (15)/ TPBi (40)/ LiF (1)/ Al
 Device B: ITO/ M_2O_3 (10)/ NPB (60)/ mCP (25)/ DPEPO: 10 wt.% **DPAc-6PyPM** (20)/ DPEPO (5)/ TPBi (40)/ LiF (1)/ Al
 Device C: ITO/ M_2O_3 (10)/ NPB (70)/ mCP (10)/ DPEPO: 20 wt.% **DPAc-TPPM** (25)/ DPEPO (10)/ TPBi (40)/ LiF(1)/ Al



Scheme S1 The structures of optimized device and chemical structures of materials employed in TADF diodes.

The device structures for single-carrier devices were based on the optimal configurations in Scheme S1. The specific device structures were provided as followed ($x=5, 10, 20$):

DPAc-4PyPM:

ITO/ M_2O_3 (10)/ NPB (60)/ mCP (15)/ DPEPO: x wt.% **DPAc-4PyPM** (20)/ mCP (15)/ NPB (60)/ M_2O_3 (10)/ Al (hole-only);

ITO/ LiF (1)/ TPBi (40)/ DPEPO (15) / DPEPO: x wt.% **DPAc-4PyPM** (20)/ DPEPO (15)/ TPBi (40)/ LiF (1)/ Al (electron-only).

DPAc-6PyPM:

ITO/ M_oO_3 (10)/ NPB (60)/ mCP (25)/ DPEPO: x wt.% **DPAc-6PyPM**: (20)/ mCP (25)/ NPB (60)/ M_oO_3 (10)/ Al (hole-only);

ITO/ LiF (1)/ TPBi (40)/ DPEPO (5) / DPEPO: x wt.% **DPAc-6PyPM**: (20)/ DPEPO (5)/ TPBi (40)/ LiF (1)/Al (electron-only).

DPAc-TPPM:

ITO/ M_oO_3 (10)/ NPB (70)/ mCP (10)/ DPEPO: x wt.% **DPAc-TPPM** (20)/ mCP (10)/ NPB (70)/ M_oO_3 (10)/ Al (hole-only);

ITO/ LiF (1)/ TPBi (40)/ DPEPO (10) / DPEPO: x wt.% **DPAc-TPPM** (20)/ DPEPO (10)/ TPBi (40)/ LiF (1)/Al (electron-only).

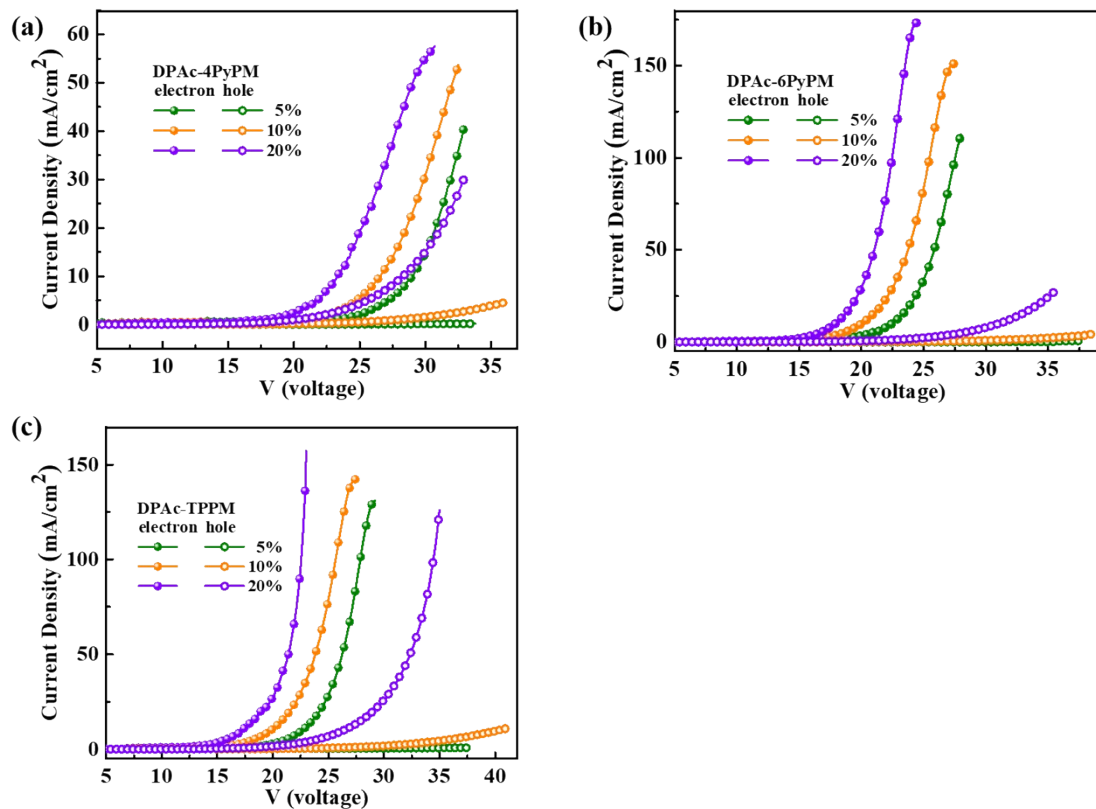


Fig. S7 Current density-voltage characteristics of hole-only and electron-only devices with different concentrations for (a) **DPAc-4PyPM**, (b) **DPAc-6PyPM** and (c) **DPAc-TPPM**.

Table S2 Recently reported TADF OLEDs based on acceptors of pyrimidine derivatives

Dopant	V_{on}^a (V)	CE^b ($cd A^{-1}$)	PE^b ($lm W^{-1}$)	EQE^b (%)	CIE^c (x, y)	Reference
DPAc-4PyPM	4.6	53.89/39.54/19.51	36.79/17.74/ 5.89	24.34/17.53/ 8.65	(0.19, 0.36)	This work
DPAc-2PyPM	4.8	35.85/18.80/ 4.45	23.45/ 7.20/ 1.04	22.42/11.27/ 2.59	(0.15,0.24)	This work
DPAc-TPPM	4.2	26.07/10.93/N.A.	19.49/ 4.90/N.A.	16.80/ 6.86/N.A.	(0.15, 0.22)	This work
2DPAc-PPM	3.6	38.10/23.50/NA	31.5/14.60/N.A.	20.80/12.40/N.A.	(0.16, 0.24)	7
2DPAc-MPM	3.6	32.0/16.50/ N.A.	27.9/11.10/ N.A.	19.0/ 9.40/ N.A.	(0.16, 0.21)	7
Ac-HPM	2.85	54.7/46.0/30.6	60.3/38.2/20.0	20.9/17.6/11.7	(0.21, 0.44)	8
Ac-PPM	2.93	49.2/43.2/29.0	52.8/33.8/17.4	19.0/16.6/11.2	(0.21, 0.44)	8
Ac-MPM	2.93	46.6/36.8/22.1	49.9/29.2/13.2	20.4/16.1/9.7	(0.19, 0.37)	8
Ac-1MHPM	3.16	46.0/26.2/11.6	45.1/26.2/11.6	24.0/19.0/11.2	(0.17, 0.28)	9
Ac-2MHPM	3.24	36.9/29.7/18.0	35.8/20.9/9.50	19.8/15.9/9.6	(0.17, 0.27)	9
Ac-3MHPM	3.25	19.9/11.7/N.A.	19.6/ 7.9/N.A.	17.8/10.4/ N.A.	(0.16, 0.15)	9
Ac-46DPPM	2.95	18.3/6.96/2.46	19.7/5.45/1.29	11.8/4.48/1.73	(0.16, 0.21)	10
Ac-26DPPM	2.87	43.5/21.2/8.61	43.5/21.2/8.61	18.6/11.9/6.34	(0.18, 0.33)	10
CzAc-26DPPM	2.87	53.9/35.3/21.9	59.2/29.3/14.1	22.8/14.9/9.28	(0.21, 0.38)	10
2SPAc-HPM	3.5	57.50/42.42/26.85	51.60/26.65/12.98	25.56/18.86/11.94	(0.18,0.34)	11
2SPAc-MPM	3.6	50.00/33.15/18.82	42.45/20.03/7.68	24.34/16.14/9.16	(0.17,0.29)	11
2SPAc-PPM	3.6	68.77/40.11/23.71	56.85/23.78/9.55	31.45/18.34/10.84	(0.18,0.32)	11
PXZPhPM	3.4	80.0/71.1/59.0	73.7/53.2/37.1	24.6/21.9/18.2	(0.32, 0.57)	12
PXZPM	3.4	65.4/58.4/46.8	60.1/43.7/28.3	19.9/17.8/14.2	(0.33, 0.57)	12
PXZMePM	3.4	71.3/63.5/49.4	68.4/47.5/29.9	22.2/19.8/15.4	(0.30, 0.56)	12

N.A.: not available. ^a Turn-on voltage (at a brightness of $1 cd m^{-2}$); ^b The order of measured value: maximum, then values at the brightness of 100 and 1000 $cd m^{-2}$. ^c Commission International de l'Eclairage coordinates recorded at $100 cd m^{-2}$.

To confirm the improved orientation to a degree, the dipole moments were calculated by TD-DFT B3LYP/6-31+G(d,p) for the lowest transition from the ground (S_0) to the excited state (S_1) and added Table S3 and Fig. S8 (Supporting Informatin). As known, the transition dipole moment is perpendicular to the direction generated photons go toward.¹³ It is found that the dipole moments are basically along their long axis in most cases. Such relatively linear dipole moments might facilitate more photons emit from devices.

Table S3 Optimized molecular structure and transition dipole moments calculated by TD-DFT B3LYP/6-31+G(d,p) for the lowest transition from the ground (S_0) to the excited state (S_1)

	DPAc-4PyPM	DPAc-6PyPM	DPAc-TPPM
P1	(0.0099, -0.0022, -0.083)	(-0.0594, 0.0165, 0.0336)	(0.0939, -0.0242, -0.0432)
P2	(-0.0014, -0.0001, 0.0584)	(-0.0103, 0.0109, 0.0347)	(0.0021, 0.0078, 0.0286)
P3	(0.5108, -0.435, 0.1112)	(-0.4206, 0.1209, -0.1349)	(0.0106, 0.0395, 0.1349)
P4	(0.0209, -0.0188, 0.0805)	(1.1862, -0.3586, -0.0239)	(-1.0911, 0.5608, -0.0153)
P5	(-0.8464, 0.6882, 0.0644)	(-0.021, -0.0288, 0.001)	(0.0122, -0.0194, -0.0878)
P_{total}	(-0.3062, 0.2321, 0.2315)	(0.6749, -0.2391, -0.0895)	(-0.9723, 0.5645, 0.0172)

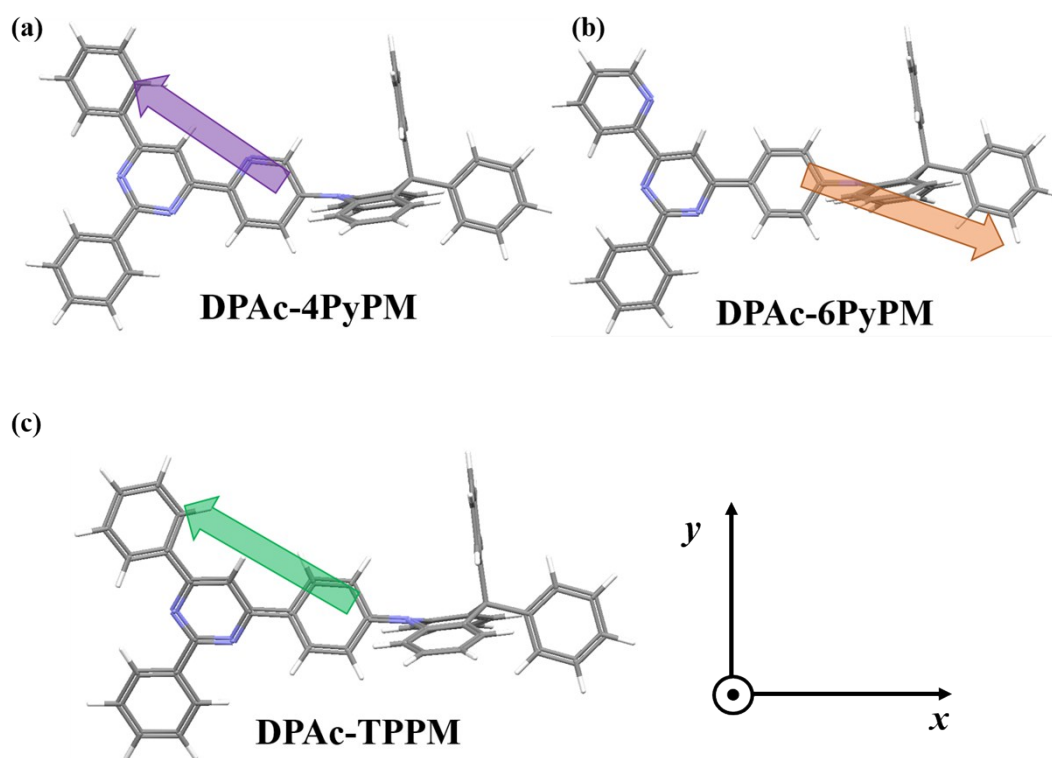


Fig. S8 The total orientations (P_{total}) of the transition dipole moments in (a) **DPAc-4PyPM**, (b) **DPAc-6PyPM** and **DPAc-TPPM**.

4-(4-bromophenyl)-2,6-diphenylpyrimidine (TPPBr): ^1H NMR (600 MHz, CDCl_3) δ : 8.74 – 8.68 (m, 2H), 8.31 – 8.25 (m, 2H), 8.20 – 8.14 (m, 2H), 7.97 (s, 1H), 7.72 – 7.66 (m, 2H), 7.61 – 7.49 (m, 6H).

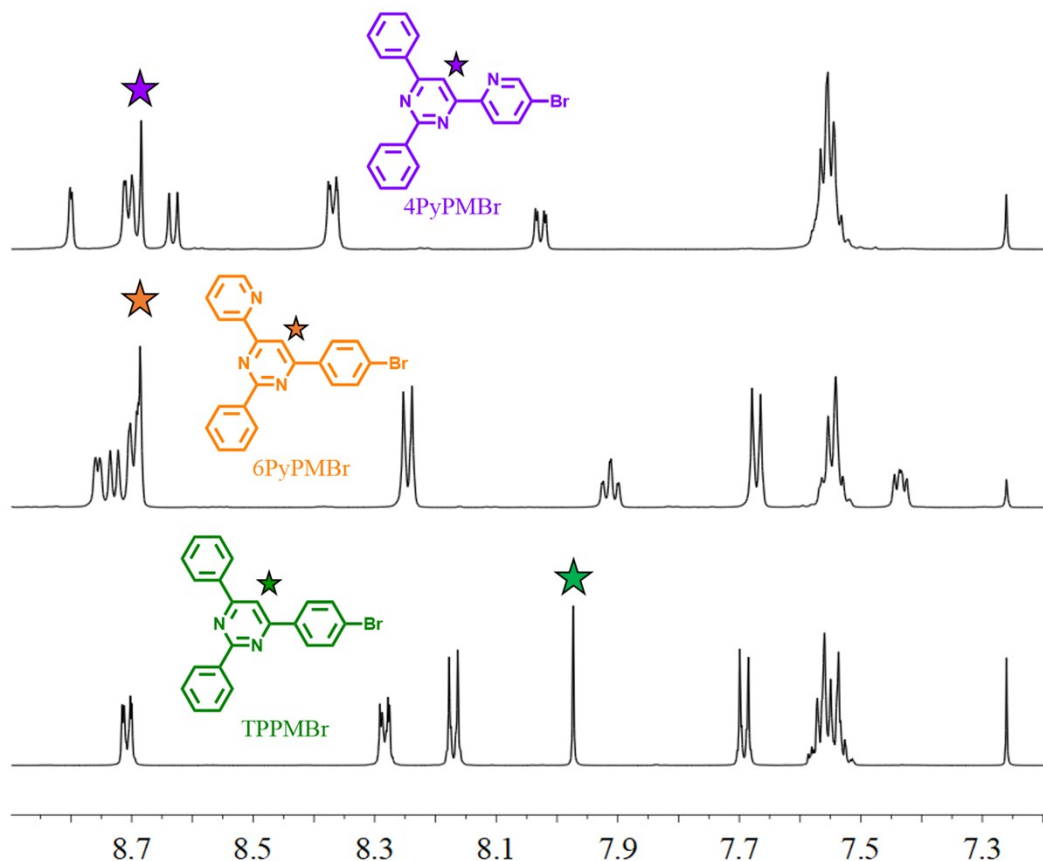


Fig. S9 ^1H NMR spectra (600 MHz) displaying the aromatic protons and signal of central pyrimidine unit. The downfield shift of pyrimidinyl proton in 4PyPMBr and 6PyPMBr are probably due to the intramolecular H-bonding interaction.

References

- 1 G. M. Sheldrick, *Acta Crystallogr A*, 2008, **64**, 112-122.
- 2 C. Rothe and A. P. Monkman, *Phys. Rev. B*, 2003, **68**.
- 3 Z. Huang, S. P. Xiang, Q. Zhang, X. L. Lv, S. F. Ye, R. D. Guo and L. Wang, *J. Mater. Chem. C*, 2018, **6**, 2379-2386.
- 4 S. Xiang, X. Lv, S. Sun, Q. Zhang, Z. Huang, R. Guo, H. Gu, S. Liu and L. Wang, *J. Mater. Chem. C*, 2018, **6**, 5812-5820.
- 5 T. Hatakeyama, K. Shiren, K. Nakajima, S. Nomura, S. Nakatsuka, K. Kinoshita, J. Ni, Y. Ono and T. Ikuta, *Adv. Mater.*, 2016, **28**, 2777-2781.
- 6 Q. Zhang, H. Kuwabara, W. J. Potscavage, S. Huang, Y. Hatae, T. Shibata and C. Adachi, *J. Am. Chem. Soc.*, 2014, **136**, 18070-18081.
- 7 I. S. Park, J. Lee and T. Yasud, *J. Mater. Chem. C*, 2016, **4**, 7911-7916.
- 8 R. Komatsu, H. Sasabe, Y. Seino, K. Nakao and J. Kido, *J. Mater. Chem. C*, 2016, **4**, 2274-2278.

- 9 R. Komatsu, T. Ohsawa, H. Sasabe, K. Nakao, Y. Hayasaka and J. Kido, *ACS Appl. Mater. Interfaces*, 2017, **9**, 4742-4749.
- 10 K. Nakao, H. Sasabe, R. Komatsu, Y. Hayasaka, T. Ohsawa and J. Kido, *Adv. Opt. Mater.*, 2017, **5**, 1600843.
- 11 B. W. Li, Z. Y. Li, T. P. Hu, Y. Zhang, Y. Wang, Y. P. Yi, F. Y. Guo and L. C. Zhao, *J. Mater. Chem. C*, 2018, **6**, 2351-2359.
- 12 K. Wu, T. Zhang, L. Zhan, C. Zhong, S. Gong, N. Jiang, Z. H. Lu and C. Yang, *Chemistry*, 2016, **22**, 10860-10866.
- 13 M. Liu, R. Komatsu, X. Y. Cai, K. Hotta, S. Sato, K. K. Liu, D. C. Chen, Y. Kato, H. Sasabe, S. Ohisa, Y. Suzuri, D. Yokoyama, S. J. Su and J. Kido, *Chem. Mater.*, 2017, **29**, 8630-8636.